Int. J. Heat Mass Transfer. Vol. 25, No. 9, pp. 1271–1278, 1982
Printed in Great Britain

0017–9310/82/091271–08 $03.00/0
Pergamon Press Ltd.

MIST COOLING OF VERY HOT TUBULES WITH REFERENCE TO THROUGH-HOLE COOLING OF GAS TURBINE BLADES

Y. MORI, K. HIJIKATA and T. YASUNAGA

Department of Physical Engineering, Tokyo Institute of Technology, Ohokayama, Meguro, Tokyo, Japan

(*Received* 23 *March* 1982)

Abstract—To develop high temperature gas turbines an advanced cooling method for turbine blades is required. This paper reports an experimental study of mist cooling of very hot tubules using air–water mist flows with particular reference to the through-hole cooling of blades. The experiments were carried out in straight and coiled tubules of 1.8 mm I.D. and local wall temperatures were measured. Firstly, it is ascertained that the heat transfer performance along the tubule axis is divided into three typical regions, namely, liquid film region, dryout region and gas-phase forced convection region. Secondly it is found that in the liquid film region the heat transfer coefficient is almost ten times higher than that without mist and no instability is observed. Thirdly, the body force gives much different heat transfer performances for the outer and inner sides of the coiled tubule.

NOMENCLATURE

B, thickness of tubule [m];
C_p, isobaric specific heat [J kg^{-1} K^{-1}];
$\mathscr{D}$, diffusion coefficient [m^2 s^{-1}];
D, diameter of spiral coil [m];
d, tubule inner diameter [m];
G, mass flow rate per unit cross-sectional area [kg m^{-2} s^{-1}];
g, gravitational acceleration [m s^{-2}];
h, thickness of liquid film [m];
i, enthalpy [J kg^{-1}];
L, latent heat [J kg^{-1}];
Nu, Nusselt number, $(\alpha d)/\lambda$;
P, total pressure [Pa];
p, partial pressure [Pa];
Pr, Prandtl number, $(\rho\nu C_p)/\lambda$;
Q, total heat supplied per unit mass to the point z;
q, heat flux [W m^{-2}];
R, gas constant [J kg^{-1} K^{-1}];
Re, Reynolds number, $(U_m d)/\nu$;
Sc, Schmidt number, $\nu/\mathscr{D}$;
Sh, Sherwood number, $(\alpha_D d)/\mathscr{D}$;
T, absolute temperature [K];
t, temperature [°C];
z, distance in the flow direction [m].

Greek symbols

α, heat transfer coefficient [W m^{-2} K^{-1}];
α_D, mass transfer coefficient [m s^{-1}];
ν, kinematic viscosity [m^2 s^{-1}];
χ, mass fraction;
σ, surface tension [N m^{-1}];
ρ, density [kg m^{-3}].

Subscripts

f, liquid film;
g, gas;
i, gas–liquid interface;
l, liquid;
m, mixed mean;
0, inlet state;
T, total of two-phase flow;
v, vapor;
w, wall.

1. INTRODUCTION

IN RESEARCH and development work on higher temperature gas turbine blades, various air or water cooling methods have been proposed, investigated and tested. Water-cooled, through-hole blades are considered more attractive and have advantages when cycles provided with regenerators and water injection in compressed air are adopted [1]. However, cooling through holes by water would have problems such as burn-out and flow instability caused by boiling.

This paper aims at an experimental investigation of the heat transfer performance of mist cooling of very hot small tubules with particular reference to gas turbine blades with cooling holes. Mist cooling of blades is similar to both air and water cooling and is useful to cycles requiring water injection into compressed air to raise the thermal efficiency of the plant. In addition to these features, a most important feature of mist cooling is its capability to control the temperature distribution of the blade by providing an adequate mist flow rate to each hole. Among mist cooling methods, cooling the blades by use of small radial through-holes is considered the most practical and appropriate. Therefore, in this paper, mist cooling of blades by through-holes is simulated by cooling very hot small tubules (electrically heated) using a mixture of air and water droplets. The fundamental heat transfer performances are then studied.

Heat transfer of two-component, two-phase flows were reviewed by Michiyoshi [2]. Correlation equa-

tions for heat transfer of mist two-component flow in pipes are described by Collier [3]. Butterworth and Hewitt [4] explain heat transfer in annular mist flows in pipes, putting importance on the turbulent liquid film but not on evaporation of the film. Many papers [5] discuss cases of high heat flux and film evaporation along the pipe inner surface for one-component, two-phase flows, but some [6] report on two-component, two-phase flows. Mist cooling by two-component, two-phase flows in strongly heated pipes has scarcely been studied.

In this paper, the heat transfer performance of two-component mist flows in very hot tubules is experimentally studied with particular reference to gas turbine blade cooling. However, in order to simulate the effects of the Coriolis force acting perpendicularly to the flow axis, a centrifugal force in a coiled tubule is used. In most flows, due to the body force working perpendicular to the flow and to the difference between the inertial forces of gas and droplet, axisymmetry of the flow is lost, and under these conditions heat transfer performances are expected to be very different from those without a body force. Considering these situations, this paper reports experimental research on two-component, two-phase flows in very hot, straight and coiled tubules with reference to through-hole cooling of high temperature gas turbine blades.

2. EXPERIMENTAL APPARATUS

In the experiments, two-phase flows of an air–water mixture were used. Figure 1 shows the experimental apparatus consisting of mixing tank, test part and power source to heat up the tubules. Water was pressurized by nitrogen at a higher pressure and supplied to the mixing tank. The flow rate of water was measured by three flow meters with the maximum range of 1 l min^{-1}. Compressed air was led to the mixing tank after its flow rate had been measured by an orifice flow meter. Details of the mixing tank (80 mm dia. and 150 mm height) are shown in Fig. 2. Air was introduced at the side of tank and water was led through a very small tubule of 0.4 mm I.D. to atomize the water. A mixture of air and water mist was then sent to the test section which consisted of a vertical tubule through a round nozzle. A portion of

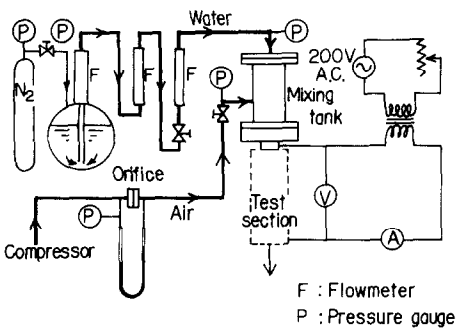

FIG. 1. Experimental apparatus.

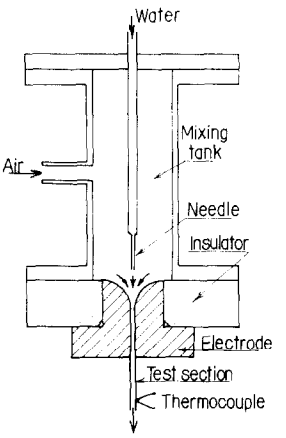

FIG. 2. Details of mixing tank.

the water appeared as droplets flowing in the main stream and the remainder as a liquid film along the inside surface of the hot tubule (stainless steel tubule, 1.8 mm I.D. and 0.1 mm thick). The round nozzle (made of copper) worked as an electrode for heating the tubule. The other electrode was attached to the lower, free end of the tubule. Three kinds of tubule were used and two of them were straight and of 150 and 300 mm length. The coiled tubule had 54 mm coil dia., 36 mm pitch and 920 mm length. Heat input to the tested tubule was calculated from the power input obtained from the heating current and the voltage drop of the tested part. When the tubule temperature was changed from 500 to 1000°C, the electric resistance varied by 10%. Therefore, the heat flux is not constant along the tube axis, but was assumed constant to simplify the experimental results.

Tubule temperatures were measured by thermocouples of 0.1 mm dia. welded directly to the tubule. The effect of the heating current on temperature readings was checked and was found to have no influence. The outside surface of tubule was not thermally insulated, but the heat loss was below 2% of heat input. Therefore, in two-phase experiments no correction for heat loss was made in the experimental results.

In the experiments with helical coils, the thermocouples were welded at the inner and outer sides of coiled tubules to measure the temperature distribution in the circumferential direction in addition to the axial direction.

3. EXPERIMENTAL RESULTS

3.1. *Experiments using straight tubules*

Figure 3 shows experimental results for temperature distributions along the pipe axis using a straight tubule of 320 mm length for air–water two-phase flow, when both the air flow rate G_g and the heat flux q were kept constant and only the water flow rate was changed. The black circles in the figure show the results for air flow and exclude the entry region. It is observed that

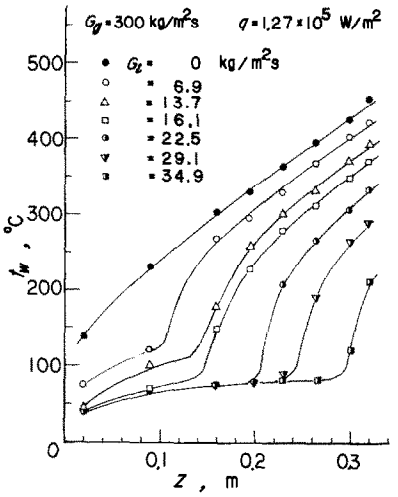

FIG. 3. Longitudinal wall temperature distribution.

the wall temperature linearly increases except at the entry region. With an increase in water flow rate, the wall temperature decreases remarkably and has a distribution different from that for air flow. Its distribution is divided into three regions, a region of slow temperature rise, followed by one of sharp temperature rise and one with a temperature gradient equal to that for air flow. For different air and water flow rates and heat fluxes, the results are also found to be divided into three regions.

These results can be explained by the change of fluid enthalpy. Denoting the mean enthalpy of the two-phase region as i_m and that at the inlet as i_{m0}, under the condition of constant heat flux we have

$$i_m - i_{m0} = \frac{4qz}{dG_T} (= Q) \tag{1}$$

where G_T is the total mass flow flux and d the inner diameter of the heated tubule. Equation (1) defines Q, which will be used later to correlate the experimental results. For a constant heat flux, Q is considered to be

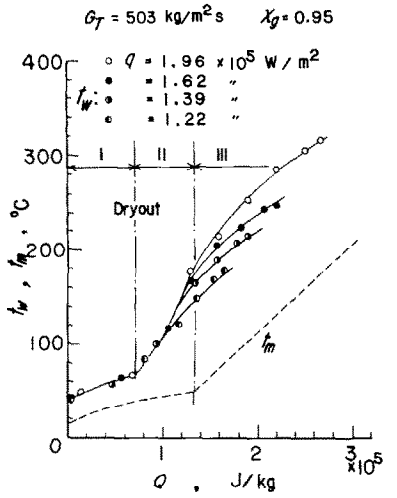

FIG. 4. Measured wall and expected mixed mean gas temperature distributions as functions of Q.

the axial distance of heating region. Defining t_m as the mixed mean temperature, the energy conservation relation is expressed as

$$[C_{pg}\chi_g + C_l(1 - \chi_g - \chi_v) + C_{pv}\chi_v] \times (t_m - t_{m0}) + L(\chi_v - \chi_{v0}) = i_m - i_{m0} = Q \tag{2}$$

where C_{pg} and C_{pv} are the isobaric specific heats for air and vapor, respectively, and C_l is that for water. χ_g and χ_v are the mass fractions of air and vapor. In a cross-section, where two phases are uniformly mixed, vapor is considered to be at a saturation state temperature t_m and we have

$$\chi_v = \frac{R_g}{R_v}\chi_g\left[\frac{p_v(t_m)}{P - p_v(t_m)}\right] \tag{3}$$

where $\chi_v < 1 - \chi_g$. R_g and R_v are the gas constants for air and vapor, respectively. P is the total pressure and $p_v(t_m)$ is the saturation pressure of vapor at t_m. When P is given, from equations (2) and (3), t_m and χ_v are obtained as χ_g is constant. After evaporation completion in the liquid phase, we have

$$\chi_v = 1 - \chi_g. \tag{4}$$

P decreases due to wall friction and acceleration caused by evaporation of liquid even though the acceleration effect is not remarkable in two-component, two-phase flows. In Fig. 4, experimental results for wall and mixed mean temperature distributions are shown against Q for the given total flow rate and air mass fraction with the heat flux as a parameter. The broken line is the calculated value of t_m for $q = 1.96 \times 10^5$ W m^{-2} and the distribution of t_m scarcely depends on the inlet pressure. Considering the behavior of t_m, the small gradient region corresponds to two-phase flow, while that of sharp gradient indicates single-phase flow. Hereafter, the abrupt turning point of t_m is called the point of completing evaporation, PCE. The wall temperature distribution is divided into three regions. In region I in Fig. 4, the distribution with gradual slope is independent of the heat flux and is followed by region II showing a sharp rise in wall temperature. In region III t_w varies with heat flux but has a gradient the same as that of t_m. The state bounding regions I and II occurs at the same value of Q and is denoted as the point of dryout PDO. PDO does not coincide with PCE because droplets flow with high speed gas and this causes a delay of mist evaporation. At the end of region II evaporation of droplets is completed.

Upstream of region I, most of the liquid phase forms a liquid film along the inner surface of the tubule, and the majority of heat added to the surface is used for evaporation, resulting in a slow rise in the wall temperature and the high heat transfer coefficient. In region II, droplets floating in the main stream evaporate by colliding with the surface or being heated by superheated air and vapor. In the following, heat transfer performances in these three regions are discussed in detail.

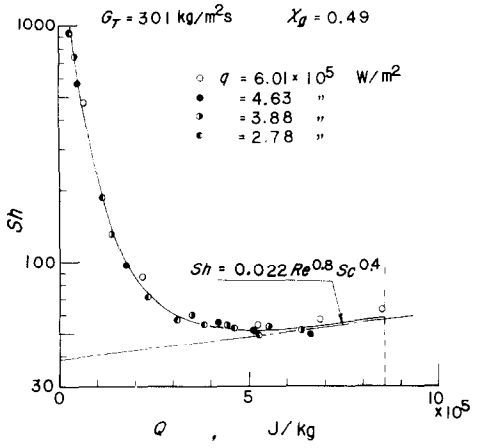

FIG. 5. Sherwood numbers in the liquid film region.

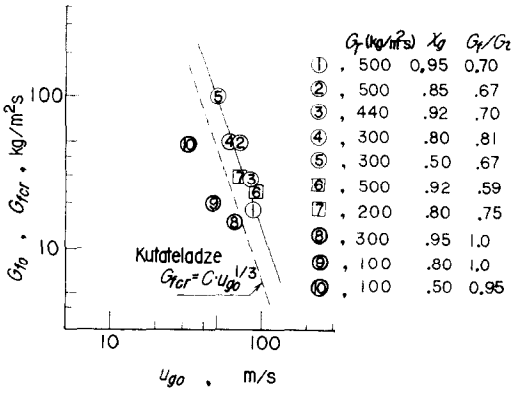

FIG. 6. The effect of inlet gas velocity on liquid film flow rate.

3.1.1. *Region I (liquid film region).* A fraction of the heat flux is used to heat the liquid film, but the remainder is used for evaporation and to heat the gas mixture. The liquid thickness h rapidly decreases with the increase in Q and is estimated by the following equation:

$$h = [2\nu_l G_f/(-\mathrm{d}P/\mathrm{d}z)]^{1/2} \tag{5}$$

where $\mathrm{d}P/\mathrm{d}z$ is the pressure gradient along the tubule axis. G_f is the liquid film flow rate and is calculated by subtracting the amount evaporated and the droplet flow rate from the total liquid flow rate. By use of the liquid thickness h calculated from equation (5), the liquid film surface temperature t_i and heat flux q_i are given approximately by

$$q_i = q - \frac{dC_l G_f}{4}\left(\frac{\mathrm{d}T}{\mathrm{d}z}\right)_w \tag{6}$$

and

$$t_i = t_w - \frac{h}{\lambda_l}\left[q - \frac{dC_l G_f}{12}\left(\frac{\mathrm{d}T}{\mathrm{d}z}\right)_w\right]. \tag{7}$$

The difference between the mass fraction of saturated vapor χ_{vi} at t_i and χ_v obtained from equations (2) and (3) is utilized to calculate the Sherwood number Sh by considering that all heat flux at the liquid surface is used for evaporation. The dependence of the diffusion coefficient on pressure and temperature is taken into account to reduce Sh. The result of Sh thus calculated is seen in Fig. 5 and shows the independence of heat flux. The chain line expresses the correlation shown by the next equation for fully developed turbulent flows. The physical properties are calculated using the mixed mean temperature.

$$Sh = 0.022\,Re^{0.8}\,Sc^{0.4}. \tag{8}$$

The fraction of heat flux used for evaporation is over 40% in the region of Q less than 5, but decreases down to several % in the region of Q greater than 5. In the region of Q greater than 8.5, the liquid film along the wall completely vanishes.

3.1.2. *Region II (mist flow region).* In this region between the points of dryout and completed evaporation, droplets are dispersed in the main stream, but the vapor near the wall is considered to be superheated. In this region a slight wall temperature fluctuation was observed.

The droplet flow rate in the gas phase is supposed to vary with the inlet atomization condition; therefore, a swirler consisting of four small vanes was provided to make droplets colliding with the wall form a liquid film. However, no shifting of the dryout point by providing the swirler was observed. This result is understood to be due to the longer entry length of the unheated part (about 20 pipe I.D.'s) and to the consequent establishment of the inlet condition to the heating section being independent of swirling.

The distance to the dryout point is considered to depend on the liquid film flow rate at the inlet of heating region. Therefore, by assuming that the liquid film flow rate G_{f0} at the inlet of heating is equal to the total evaporated vapor flow rate, the correlation between G_{f0} thus calculated and the gas velocity at the inlet is shown in Fig. 6. The number in the figure is the number of experimental run.

Kutateladze [7] suggested the following equation for the critical flow rate of annular flowing-down liquid film in a vertical pipe:

$$\frac{G_{fcr}d}{4\rho_l\nu_l} = \left[\frac{54}{u_g}\left(\frac{g\sigma\rho_l}{\rho_g^2}\right)^{0.25} \times \left(\frac{\sigma^3}{\nu_l^4\rho_l^3 g}\right)^{0.0365}\left(\frac{\nu_l}{\nu_g}\right)^{0.24}\right]^3 \tag{9}$$

where σ is the surface tension. Equation (9) is expressed in Fig. 6 by the broken line. The left side of this line is the stable region. The experimental points shown in Fig. 6, excluding the runs 8, 9 and 10, lie on a straight line which has the power of -3, being the same as equation (9), but has a liquid film flow rate larger than that given by equation (9). In the runs 8, 9 and 10, the dryout point and evaporation completion point coincide with each other and the whole liquid flows as the liquid film. These runs have smaller G_{f0} than other

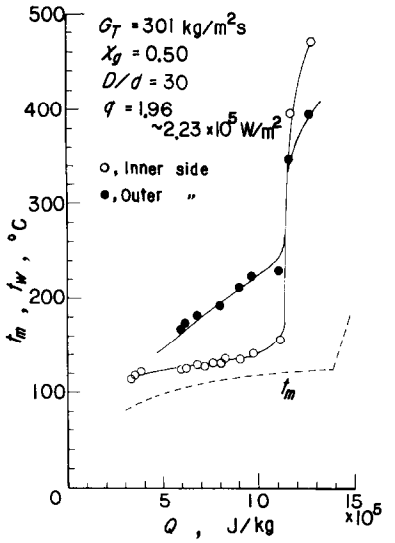

FIG. 7. Measured wall and expected mixed mean gas temperature distributions of coiled tubule.

runs, and are in the stable region. It is concluded that when the liquid flow rate is smaller than the critical value, the liquid film is stable and all liquid is considered to flow as liquid film. The experimental results also explain that the liquid film is more stable than expected by equation (9) due to the surface tension effect on the film flow along the inner surface of a smaller tubule.

3.1.3. *Region III (single-phase region).* Downstream of the evaporation completion point, fully-developed convective heat transfer in the vapor and air mixture is established. The correlation of Nusselt numbers Nu obtained in this region against Reynolds number Re_{gv} of the air–vapor mixture agrees with the relation reported [8], which includes the correction term for the physical property variation with temperature.

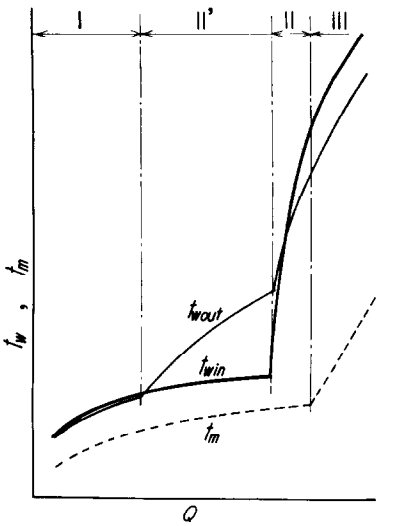

FIG. 8. Typical wall and mixed mean gas temperature distributions showing the four regions for a coiled tubule.

3.2. *Experiments using a coiled tubule*

In the radial rotating hole of a gas turbine blade, in addition to a centrifugal force of about 10^4 g, there is a large Coriolis force which works on the flow in it. In order to study the effect of a force acting perpendicularly to the flow direction, such as a Coriolis force, a centrifugal force acting on a flow in a coiled tube can be substituted. In this simulation experiment, a coiled tubule of 1.8 mm I.D. having a 54 mm diameter of curvature was used. The centrifugal force is about 3 × 10^3–10^4 g. The experimental procedure used was the same as that for the straight tubules. Data for wall temperature distributions are shown in Fig. 7. The broken line expresses the mixed mean temperature and the open and solid circles indicate the surface temperatures of the inner and outer sides of the coiled tubule, respectively. Based on data such as those shown in Fig. 7, the typical and schematic temperature distributions of the inside and outside walls and the mixed-mean main stream are shown in Fig. 8. The distributions are divided into four regions, regions I, II and III having almost similar performances to those without a body force, but with a new region, region II', appearing in addition expressing the effects of the body force. In region I, a liquid film covers the inner and outer side walls of tubule, and consequently both wall temperatures are the same. With the increase of Q, at the critical value of Q bounding regions I and II', dryout is considered to occur at the outer wall and in region II', the outer wall temperature increases more rapidly than that of the inner wall. The reason why the rise of the outer wall temperature is not sharp enough is explained later. At the next critical value of Q bounding regions II' and II, dryout occurs even at the inner-coil side of the tubule. The whole tubule wall is dry but droplets exist in the main stream. In region II, the temperature rise of the inner side is more rapid than that of the outer. Consequently, the inner wall temperature becomes higher than the outer wall temperature in the latter part of region II and in the following region, region III. In region III, the temperature rises similarly at the inner and outer sides and single phase flow is established. These performances differ for the inner and outer sides of tubule due to the secondary flow in the main stream caused by the centrifugal force. The smaller distance between the dryout and evaporation completion points in the straight tubule is explained by the violent collision of droplets in the

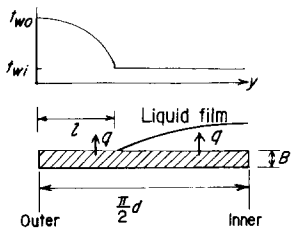

FIG. 9. Schematic surface temperature profiles in the circumferential direction of a coiled tubule.

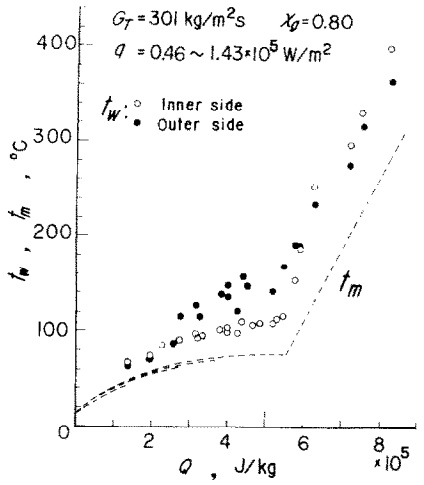

FIG. 10. Measured wall and expected mixed mean gas temperatures as functions of Q for a coiled tubule.

main stream with the wall caused by the secondary flow. The earlier dryout along the outer wall is also reported by Kosegi [9] for one-component, two-phase flow in coiled tubes. This phenomenon is understood to be caused by the film thickness being thicker at the inner side due to the film motion to the coil inner side induced by the shearing stress of the secondary flow. In other words, liquid uniformly covering the inside wall of tubule at the entry region is caused to flow to the coil inner side by the secondary flow and the former dryout occurring at the outside.

In region II, it should be noted that the temperature rise of the outer wall after dryout is not so remarkable compared with that for the straight tubule. Kosegi explains this by the collision of droplets in the main stream with the outer wall, but this fact is explained here by thermal conduction in the circumferential direction of the tubule. This is partly due to the small tubule diameter and the short circumferential distance between the inner and outer sides (about 3 mm). In the upper part of Fig. 9, a wall temperature

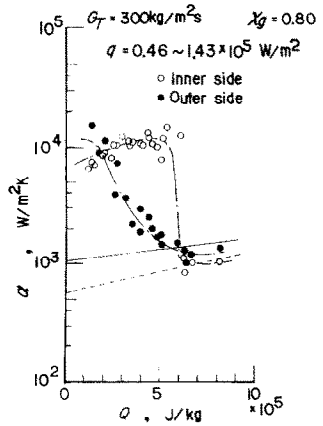

FIG. 11. Effective heat transfer coefficient of mist cooling in a coiled tubule.

distribution is shown against the circumference distance from the outer side where t_{w0} is the outer wall temperature and t_{wi} is that of the inner wall. In the lower part the liquid film along the thermally conductive wall is schematically shown. The part covered by the liquid film is maintained at temperature t_{wi} and heat flux q is applied at the wall. The solution of the conduction equation gives the following relation by assuming the difference between the film surface temperature and the mixed mean temperature of the main stream to be very small in comparison with q/α:

$$[(t_w)_{y=0} - t_{wi} = \Delta t[1 - \{\cos h[(\alpha l)/(B\lambda_w)]\}^{-1}] \quad (11)$$

where B and λ_w are the thickness and the thermal conductivity of the wall, respectively. α is the heat transfer coefficient of the dry surface. The numerical value by equation (11) for Fig. 7 at the dryout point of the inner wall, that is, $Q \simeq 11.5 \times 10^5$ J kg^{-1} and $l = (\pi d)/2$ in equation (11) is about 120°C and well explains the result shown in Fig. 7.

Figure 10 shows the experimental results for the temperature distributions for the smaller liquid-phase flow rate with the same total flow rate as that of Fig. 8. In the case of Fig. 10, as the liquid flow rate is much smaller, region II shown in Fig. 8 does not exist.

The effective heat transfer coefficient is calculated by use of the measured wall temperature and the assumed mixed mean temperature of the main stream and is shown in Fig. 11. The broken line indicates that for fully developed turbulent convective heat transfer of gas flow in straight pipes [8], the solid line that for turbulent heat transfer in coiled tubes [10]. The physical properties are calculated using mean temperature. In the smaller Q region, the heat transfer coefficient for the outer side is higher than that for the inner side, but decreases rapidly with the increase in Q. On the contrary, the heat transfer coefficient of the inside wall down to the dryout point is about ten times higher than that for gas flows. This is due to evaporation of the liquid film. Nusselt numbers obtained for a large air flow rate after the dryout of the inner side wall, once the fully developed state is well established, are shown in Fig. 12, with the physical properties corrected. The broken and solid lines are the same as those in Fig. 11. The data for the outer side are a little higher than those for the inner side, as predicted by Pratap [11].

4. CONCLUSION

With reference to through-hole cooling of gas turbine blades, experimental research on mist cooling of hot straight and coiled tubules was conducted using air–water mist flows, and the following conclusions were obtained:

(1) Most of the water flows as a water film along the inside surface when water is atomized and injected in the air flow. Heat transfer in the region down to the dryout point of liquid film is mainly controlled by film evaporation.

(2) When the liquid film vanishes the dryout point is

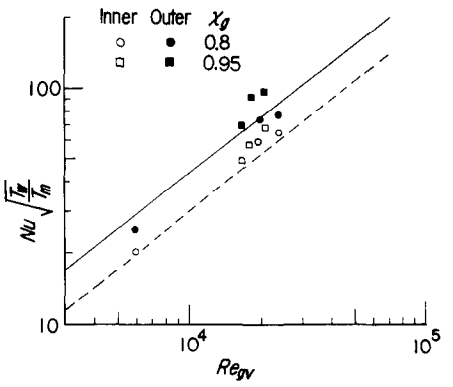

FIG. 12. Nusselt numbers of gas flow in a hot coiled tubule.

upstream of evaporation completion point of the main stream. The flow rate of liquid film at the inlet is tightly connected with the critical liquid flow rate of annular flow.

(3) The heat transfer coefficient downstream of the evaporation completion point is well correlated by that of convective gas-phase flows in straight or coiled pipes.

(4) The secondary flow in the main stream in coiled tubules causes an earlier dryout at the outer wall than at the inner wall, and heat transfer performances (in the case when the outer wall is dry and the inner wall is covered by liquid film) are well explained by thermal conduction in the circumferential direction of wall.

(5) The effective heat transfer coefficient is about ten times higher than that for air flows in the coiled tubule. Consequently, the mist cooling is considered effective for through-hole cooling of gas turbine blades.

REFERENCES

1. N. Gasparovic and J. G. Hellemans, Gas turbines with heat exchanger and water injection in the compressed air, *Combustion* **44**, 32–40 (1972).
2. I. Michiyoshi, Two-phase two-component heat transfer, *Proc. 6th Int. Heat Transfer Conf.*, Toronto, Vol. 6, pp. 219–233 (197).
3. J. G. Collier, *Convective Boiling and Condensation*. McGraw–Hill, London (1972).
4. D. Butterworth and G. F. Hewitt, *Two-Phase Flow and Heat Transfer*. Oxford University Press, Oxford (1977).
5. F. Mayinger and H. Langner, Post-dryout heat transfer, *Proc. 6th Int. Heat Transfer Conf.*, Toronto, Vol. 6, pp. 181–198 (1978).
6. R. H. Pletcher and H. N. McManus, Heat transfer and pressure drop in horizontal annular two-phase component flow, *Int. J. Heat Mass Transfer* **11**, 1087–1104 (1968).
7. S. S. Kutateladze, *Problems of Heat Transfer and Hydraulics of Two-Phase Media*. Pergamon Press, London (1969).
8. D. M. McEligot, C. W. Ormand and H. C. Perkins, Internal low Reynolds-number turbulent and transitional gas flow with heat transfer, *Trans. Am. Soc. Mech. Engng*, Series C, *J. Heat Transfer* **88**, 239–245 (1966).
9. M. Kosegi, H. Nariai, T. Furukawa and K. Kurosu, Study on curved tube steam generator, *J. Japan Soc. Mech. Engrs* **73**, 538–546 (1970).
10. Y. Mori and W. Nakayama, Study on forced convective heat transfer in curved pipes, *Int. J. Heat Mass Transfer* **10**, 37–59 (1967).
11. V. S. Pratap, Flow and heat transfer in curved ducts, Ph.D. thesis, University London HTS/75/25 (1975).

REFROIDISSEMENT PAR BROUILLARD DE TUBULES TRES CHAUD AVEC REFERENCE AU REFROIDISSEMENT PAR SOUFFLAGE DES AUBES DE TURBINE A GAZ

Résumé—Pour développer les turbines à gaz à haute température, est nécessaire une methode performante de refroidissement des aubes. On fait l'étude expérimentale du refroidissement par brouillard de tubules très chauds en utilisant des écoulement de brouillard d'eau avec référence au refroidissement par soufflage. Les expériences sont faites avec des tubules droit ou courbes de 1,8 mm de diamètre intérieur et on mesure les températures pariétales locales. Il est certain que le transfert thermique le long de l'axe du tubule est divisé en trois types : la région du film liquide, celle de l'assèchement et celle de la convection forcée en phase gazeuse. D'autre part dans la région du film liquide, le coefficient de transfert thermique est à peu près dix fois plus grand que celui sans brouillard et on n'observe pas d'instabilité. Enfin, la force de volume donne des performances thermiques plus différentes pour les cotés externe et interne du tubule courbe.

NEBELKÜHLUNG VON SEHR HEISSEN RÖHRCHEN IM HINBLICK AUF DIE INNENKÜHLUNG VON GASTURBINENSCHAUFELN

Zusammenfassung—Um Hochtemperatur-Gasturbinen entwickeln zu können, braucht man unbedingt ein fortschrittliches Kühlverfahren für die Turbinenschaufeln. In dieser Arbeit wird über eine experimentelle Studie zur Nebelkühlung sehr heißer Röhrchen mit Hilfe von Luft–Wasser-Nebelströmungen mit besonderem Bezug auf die Innenkühlung von Schaufeln berichtet. Die Versuche wurden mit geraden und Spiralröhrchen von 1,8 mm innerem Durchmesser durchgeführt und die örtlichen Wandtemperaturen gemessen. Erstens wurde festgestellt, daß für den Wärmeübergang entlang der Achse der Röhrchen drei typische Bereiche zu unterscheiden sind, nämlich der Bereich des Flüssigkeitsfilms, der Austrocknungsbereich und der Bereich erzwungener Konvektion der Gasphase. Zweitens wurde gefunden, daß im Bereich des Flüssigkeitsfilms der Wärmeübergangskoeffizient ungefähr zehn mal größer ist als ohne Nebel und daß keine Instabilität zu beobachten ist. Drittens zeigte sich, daß durch die Trägheitskräfte sehr unterschiedliche Werte des Wärmeübergangs an der Innen- und Außbenseite der Spiralröhrchen auftreten.

ИССЛЕДОВАНИЕ ВОЗДУШНО-КАПЕЛЬНОГО ОХЛАЖДЕНИЯ СИЛЬНО НАГРЕТЫХ ОТВЕРСТИЙ В ПРИЛОЖЕНИИ К СКВОЗНОМУ ОХЛАЖДЕНИЮ ЛОПАТОК ГАЗОВЫХ ТУРБИН

Аннотация—Для дальнейшей разработки высокотемпературных газовых турбин настоятельно необходим новый метод охлаждения турбинных лопаток. В работе проведено экспериментальное исследование воздушно-капельного охлаждения сильно нагретых отверстий в приложении к сквозному охлаждению турбинных лопаток. Эксперименты проводились с прямыми и спиральными трубочками с внутренним диаметром 1,8 мм. Измерялись локальные значения температуры стенок. Во-первых установлено, что интенсивность теплопереноса вдоль оси трубки характеризуется тремя диапазонами: областью жидкостной пленки, областью критического теплового потока и газофазной областью с вынужденной конвекцией. Во-вторых, что в области с жидкостной пленкой коэффициент теплопереноса почти в десять раз выше, чем без воздушно-капельной взвеси, и неустойчивость отсутствует. В-третьих, что интенсивность теплопереноса на внешней и внутренней поверхностях спиральной трубочки сильно отличается из-за влияния массовых сил.